International Symposium
On Turbulence and Shear Flow
Phenomena (TSFP-9)
June 30 - July 3, 2015 *Melbourne, Australia*

PROPER ORTHOGONAL DECOMPOSITION ANALYSIS OF A PUFF IN A PIPE

David Moxey[1], Yuri Feldman[2], Paris Perdikaris[3], Joseph Insley[4], Alexander Yakhot[2], Spencer Sherwin[1], George Karniadakis[3]
[1]Department of Aeronautics, Imperial College London, South Kensington Campus, London SW7 2AZ, UK
[2]Department of Mechanical Engineering, Ben-Gurion University, Beersheva 84105, Israel
[3]Division of Applied Mathematics, Brown University, Providence, RI 02912, USA
[4]Argonne Leadership Computing Facility, Argonne National Laboratory, Argonne, IL 60439, USA

ABSTRACT

We have performed direct numerical simulations of transitional turbulence in pipe flow for Re=2,250. The results confirm the existence of a spatio-temporal intermittency when turbulence is localized in a puff convected downstream. To analyze the turbulence, we follow a turbulent puff by a 3D moving-window centered at the location of the maximum total energy of transverse (turbulent) motion. The flow field data collected over 6,000 time instances (snapshots) have been analyzed by Proper Orthogonal Decomposition (POD) and used for identifying vortical structures. The presence of large-scale structures in a puff has been found by time-averaging of the cross-sectional turbulent velocity field and confirmed by POD analysis and by applying the Q- and λ_2-criteria.

PUFFS IN TRANSIENT PIPE FLOW

Forty years ago, experiments conducted in a pipe for mixed laminar-turbulent flows at 2,000 <Re <2,700 revealed turbulent regions convected downstream (see Wygnansky & Champagne, 1973 and Wygnansky *et al.*, 1975). The authors called these regions *puffs*. It was found that, depending on the flow conditions, puffs grow, split and even recombine. A single puff at $Re \approx 2,280$ and four puffs at Re $\approx 2,630$ were experimentally observed in Wygnansky *et al.* (1975). The flow in pipe becomes fully turbulent at low Reynolds number $Re \approx 3,000$. Recently, the splitting events were studied both numerically and experimentally (Moxey & Barkley, 2010; Avila *et al.*, 2011). Moxey & Barkley (2010) carried out extensive direct numerical simulations in pipes of variable lengths up to 125 diameters to investigate the nature of transitional turbulence in pipe flow.

One of the main conclusions of Avila *et al.* (2011) is that isolated (or equilibrium) puffs as seen by Wygnansky *et al.* (1975) do not exist. After some finite lifetime governed by a super-exponential distribution, a given puff will either decay or split. To understand the role that puffs play in the transition process, a detailed understanding of the mechanism that dictates how a puff grows and splits is therefore necessary.

We note that although puffs will eventually split or decay, near the critical Reynolds number their lifetime is extremely high with order around 10^8 time units. Consequently, studying the properties of long-time transient puffs around these Reynolds numbers, using highly resolved numerical experimental studies, will provide further insight in the laminar-turbulent transition in a pipe.

The aim of the present paper is to analyze the turbulent velocity field inside a long-time transient puff travelling through a pipe. For this purpose, we resumed the long time DNS described in Moxey & Barkley (2010) for Re = 2,250 in axially periodic pipes of length L = 25D and 50D. The approximate length of a single puff is about 25D. For longer pipes, the flow is intermittent with irregular alternation of turbulent and *completely* laminar regions. There is no clearly distinguished interface between the turbulent and laminar zones neither near the leading edge, nor near the trailing edge of a puff. Additionally, in long pipes, turbulent-laminar states exhibit complex spatio-temporal dynamics, with puffs splitting and merging as the simulation evolves. To ensure the existence of a single puff, we analyze the data obtained for a pipe with $L = 25D$.

In Moxey & Barkley (2010), the magnitude of the transverse velocity $q(x,y,z,t) = \sqrt{u^2+v^2}$ was used as an informative and easily accessible quantity to indicate the existence of turbulence in the flow; (x,y) are in-plane transverse coordinates, z is the axial coordinate. For laminar flow, there is no transverse motion, $u = v = 0$ and, consequently, $q = 0$. Figure 1 illustrates the approach of a moving-window (mw) of the width $\pm 2D$ centered around the location where $q = q_{max}$. In this paper, for each temporal snapshot, we identify a cross-section (z-location), wherein the *cross-sectional mean* value of $< q^2 >$ is maximal. Then, we construct a 3D-window of the width approximately $\pm 2D$ centered around this location.

We use the spectral element code *Semtex* (Blackburn & Sherwin, 2004), with the same mesh and polynomial order as used in Moxey & Barkley (2010) and 384 Fourier modes in the axial direction. Therefore, the moving-window consists of 63 cross-sectional slices, hereafter, denoted as S1, S2,..., S63; $< q^2 >$ is maximal at S32. In the time-evolving frame, this moving-window aims to observe the moving puff in a "quasi-Lagrangian" sense, defining the 3D subdomain wherein the data analysis is carried out. We collected 6,000 snapshots of the flow field, with a time interval of $\Delta T = 0.2$ time units between snapshots. Therefore, a puff, moving in the pipe with a velocity slightly smaller than the bulk velocity, convects approximately 1,200D or 48 pipe lengths.

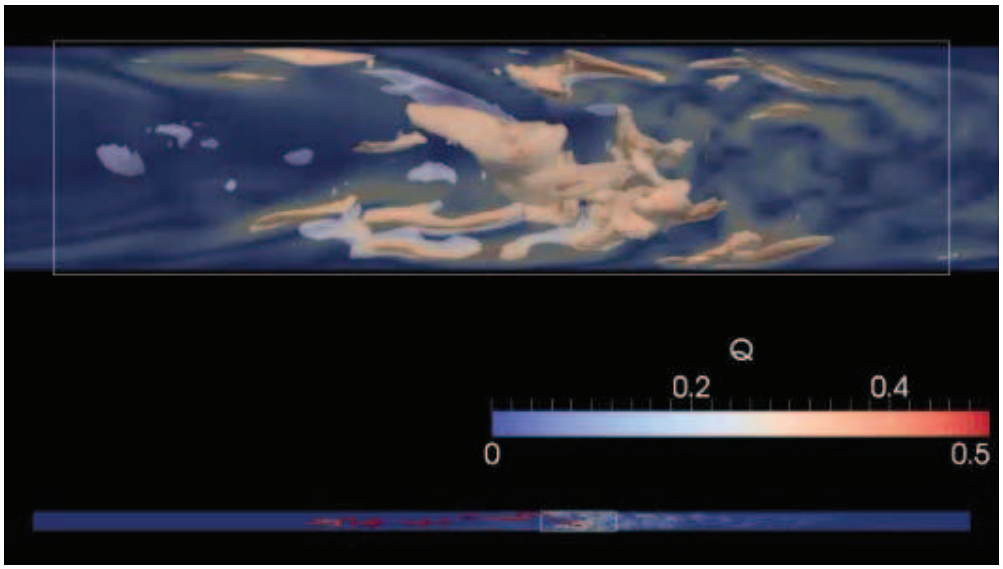

Figure 1. *Bottom:* 2D visualization of flow in a straight pipe of $L = 50D$ at Re=2,250: contour of the instantaneous transverse velocity magnitude q and the space-time trace of its maximal value $q_{max}(x,y,z,t)$ (in *red*); a moving-window of the width $\pm 2D$ centered around $q_{max}(x,y,z,t)$. *Top:* 3D iso-surfaces of the instantaneous transverse velocity magnitude q in a zoomed-in moving-window.

In this paper, we focus on cross-sectional (in-plane) fields when there is no mean flow for fully-developed flow in a pipe. We decompose the velocity as fluctuating and coherent parts

$$\mathbf{u}(\mathbf{x},z,t) = \mathbf{u}'(\mathbf{x},z,t) + \mathbf{u}_c(\mathbf{x},z,t), \tag{1}$$

where $\mathbf{u} = (u_r, u_\theta)$ and $\mathbf{x} = (r,\theta)$. Assuming that in the transitional flow at hand organized (coherent) large-scale structures exist, at each z-location $\overline{\mathbf{u}'}(\mathbf{x},z,t) = 0$ but $\overline{\mathbf{u}_c}(\mathbf{x},z,t) \neq 0$; a bar denotes the time-averaging over 6,000 snapshots.

The developing transverse (cross-sectional) motions inside the puff play a special role in the onset of turbulence. In Figure 2, we show 3D iso-surfaces of the time-averaged transverse velocity components, $\overline{u_r}$ and $\overline{u_\theta}$ inside the puff. First of all, it is striking that prints of contours on the trailing edge section (S1) have a periodic structure around the circumference of the pipe. Further downstream, the periodicity breaks down. Figure 3 shows separately S1, S32 and S63 - the trailing edge, middle and leading edge cross-sections, respectively, of the moving window. In the caption to Figure 3, we deliberately use the notation $\overline{u_r}$ in favor of the decomposition (1). The near-wall periodic waviness clearly indicates the existence of low-speed fluid ejection ($\overline{u_r} < 0$) at the wall. On the other hand, the high-speed fluid flows away from the center towards the wall ($\overline{u_r} > 0$). This is the mechanism of developing the well-known near-wall hairpin-like vortices as the onset of turbulence. Similar patterns have been found in van Doorne & Westerweel (2009) from particle image velocity measurements.

In conclusion of this introductory part, the time-averaged radial velocity pattern suggests the presence of organized large-scale structures in the puff (Fig. 3a).

POD OF THE EQUILIBRIUM PUFF

The idea of POD is to generate an orthogonal set of basis temporal and spatial modes which span an ensemble of data (snapshots), collected experimentally or from a numerical procedure of an evolving dynamical system. In computational fluid dynamics, the POD has been applied to study most DNS results of benchmark tests of fully turbulent flows at relatively high Reynolds numbers.

The POD eigenvalue spectrum shows the significance of an individual mode in terms of energy. Consequently, there is an energy transfer from low index POD modes to higher modes and this transfer is local; energy transfers among the neighboring POD modes. In addition, all known POD eigenvalue spectra of developed turbulent flows in the literature span at least over 6-8 orders of magnitude.

We employ the following decomposition of the velocity field: $u(\mathbf{x},t)$

$$u(\mathbf{x},t) = \sum_{j=1}^{M} a_j(t)\phi_j(\mathbf{x}), \tag{2}$$

where $\mathbf{x} = (x,y,z)$ or $\mathbf{x} = (r,\theta,z)$, and $\phi_j(\mathbf{x})$ and $a_j(t)$ are the j-th orthogonal spatial and temporal modes, respectively. The POD procedure yields the eigenfunctions $\{\phi_j\}$, which form the expansion basis in the above expression. Here, we implement the method of snapshots introduced by Sirovich (1987) to obtain the eigenfunctions and corresponding eigenvalues. Consider the collection of M data snapshots, $\{\mathbf{u}^k\}_{k=1}^{M}$, where $\mathbf{u}^k$ is a vector containing the velocity field at time t_k for all $\mathbf{x} = \mathbf{x}_1,\ldots,\mathbf{x}_N$, that is, the elements of the $M \times N$ (time$\times$space) matrix $\mathbf{u}^k$ are

$$u_i^k = u(t^k,\mathbf{x}_i), \quad i = 1,2,\ldots,N, \;\; k = 1,2,\ldots,M. \tag{3}$$

These snapshots are used to compute the POD basis vectors, which yield a representation of the data that is optimal in the

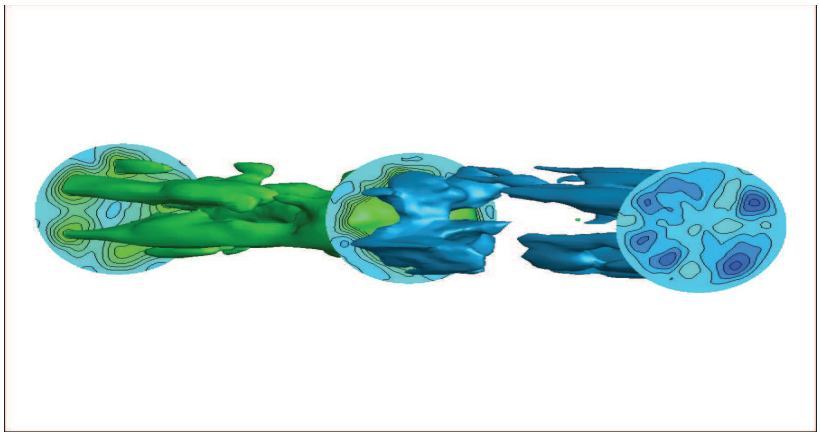

Figure 2. 3D iso-surfaces of the time-averaged transverse u_r-velocity in a moving-window of the width $\pm 2D$; at each time instance, t, the window is centered around the cross-section S32 with $< q^2(x,y,z,t) >=< q^2 >_{max}$ $(z = S32,t)$; the brackets indicate cross-sectional averaging, the cross-sections S1, S32 and S63 with u_r-contours are shown.

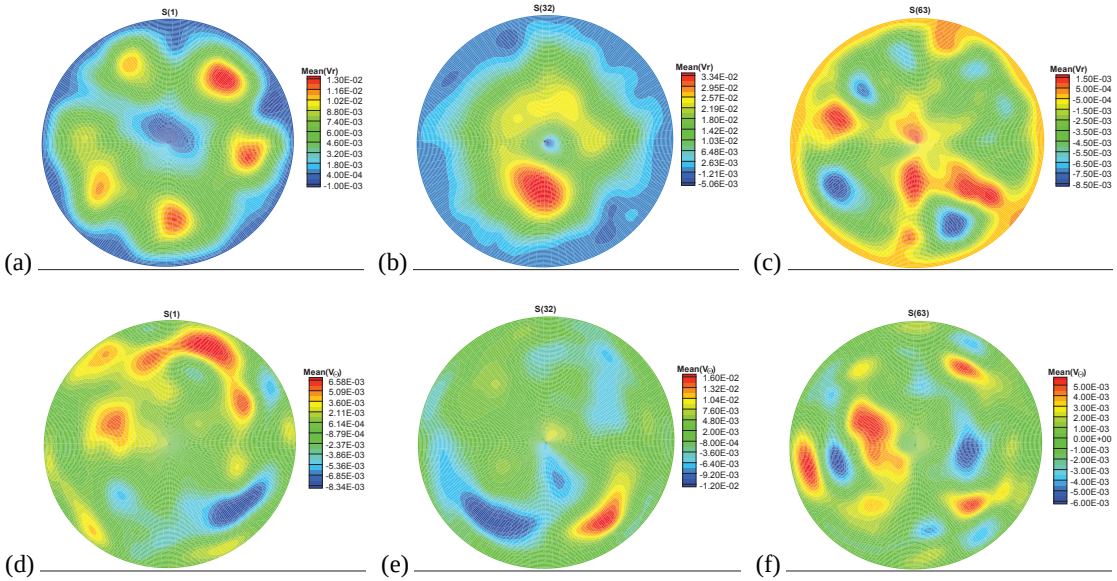

Figure 3. Contours of the time-averaged transverse velocity components, $\overline{u_r} = \overline{u_{cr}} = \text{Mean}(V_r)$ (a-c), $\overline{u_\theta} = \overline{u_{c\theta}} = \text{Mean}(V_\theta)$ (d-f). S1, S32 and S63 - the trailing edge, middle and leading edge cross-sections, respectively, of a moving window.

sense that, for any given basis size, the L_2 norm of the error is minimized. This is equivalent to solving the eigenvalue problem $\mathbf{CA} = \Lambda\mathbf{A}$, where the eigenvectors a_j (columns of the $M \times M$ matrix $\mathbf{A}$) represent the temporal modes, Λ is a diagonal $M \times M$ matrix of the eigenvalues λ_j. Here, $\mathbf{C}$ is a correlation $M \times M$ matrix computed by multiplying the snapshots $M \times N$ matrix $\mathbf{u}^i$ by its transpose $(\mathbf{u}^i)^T$ and normalizing by the number of snapshots M. Owing the orthogonality of the temporal basis eigenvectors a_j, j-th POD spatial basis vector $\phi_j(\mathbf{x})$ is found from the expansion (2): $\phi_j(\mathbf{x}) = \sum_{k=1}^{M} a_j^k \mathbf{u}^k$, $j = 1,2,\ldots,M$, where a_j^k denotes the k-th element of the j-th eigenvector a_j. Finally, the velocity field reconstructed by truncated number $N_m < M$ of modes is computed from:

$$\widetilde{\mathbf{u}}^k = \sum_{j=1}^{N_m} a_j^k \phi_j, \qquad (4)$$

for every $k = 1,2,\ldots,M$.

The POD expansion has a hierarchical structure, which means each energetic process is attributed to a certain spatio-temporal mode and each spatio-temporal mode adds its basic flow structure to the total turbulent flow field. As follows from the definition of the auto-correlation matrix $\mathbf{C}$, the magnitude of the j-th eigenvalue, λ_k, estimates the contribution of the k-th mode to the total energy, that is, $E_{total} = \sum_{k=1}^{M} \lambda_k$.

In this study, we apply POD analysis to the data set collected inside a moving window (mwPOD). In this sense, the suggested mwPOD approach invites an obvious question. Indeed, it is not a Lagrangian approach, we do not follow the same fluid particles. We "trace" a moving puff identifying its location at each snapshot by a condition ($< q^2 >_{max}$) and, even if the time interval between snapshots is chosen reasonably small, it is set quite arbitrarily. One can claim that such conditionally sampled ensemble of data sets is not governed by a dynamic system (Navier-Stokes) or, in other

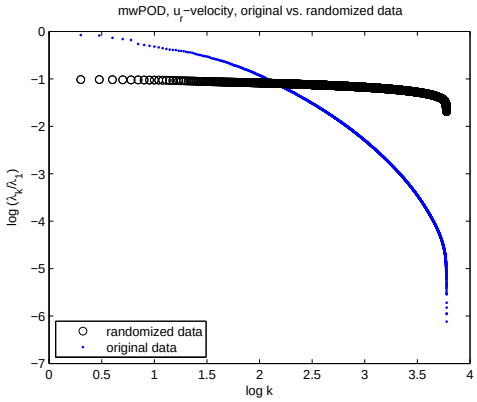

Figure 4. Eigenvalue spectrum, original vs. randomized data.

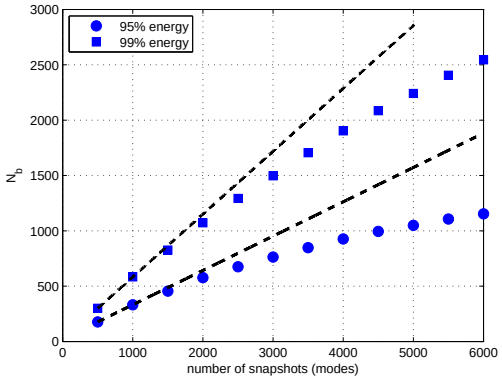

Figure 6. Number of modes to capture 95% and 99% of the energy.

Table 1. Relative u_r-velocity energy accumulated in the first N_m POD modes, $E_m/E_{total} = \sum_{k=1}^{N_m} \lambda_k / \sum_{k=1}^{6000} \lambda_k$

N_m	2	4	10	100	500
E_m/E_{total}	0.035	0.065	0.130	0.523	0.843

words, the moving-window snapshots are an ensemble of uncorrelated data. To check, we performed a simple test: POD analysis of data collected over the moving window; then, at each snapshot, the 3D data was randomly shuffled and the POD analysis repeated. Figure 4 shows the test result. First, the eigenvalue spectrum of the original data shows clear signs of a typical POD analysis: eigenvalues span more than six orders of magnitude. On the other hand, the spectrum of randomly rearranged (dynamically uncorrelated) data is rather flat showing the energy decrease by one-and-a-half order of magnitude only.

We have performed mwPOD analysis of the radial (u_r) and circumferential (u_θ) velocity components. In Figure 5, we show the eigenvalue spectra of velocity components for different number of snapshots. For 6,000 snapshots (modes), the spectrum spans over about 6.5 orders of magnitude.

The number of basis modes required to capture a specified percentage of the turbulent energy is denoted N_b and indicates the total number of degrees of freedom of the flow at hand. Figure 6 shows N_b to capture 95% and 99% of the total energy.

The number of basis modes should be asymptotically achieved with increasing the number of snapshots. Our results show the evidence of the asymptotical tendency for 95% ($N_b \approx 1,200$), but do not allow conclusions about N_b for 99%. This can be due to the moving-window (test volume) size and is the subject of further study. In Duggleby *et al.* (2007), the number of basis modes to capture 90% and 94% of the energy is 2,763 and 5,000, respectively.

In Figure 7, we show the color map of u_r-velocity reconstructed by different number of mwPOD modes. Already the first four modes strikingly reproduce the pattern similar to the entire field shown in Figure 3a. In Table we present the relative energy accumulated in the first N_m mwPOD modes. It is noteworthy, that the first four modes accumulate only 6.5% of the total energy. Apparently, the structure that we see in Figure 3a is formed even by the first four POD modes, while other modes "drop" energy inside.

Q- AND λ_2-CRITERIA FOR VORTICAL MOTION

An "eddy" (structure) is defined as a region with a positive second invariant $Q = \frac{1}{2}\left(\|\mathbf{\Omega}\|^2 - \|\mathbf{S}\|^2\right) = -\frac{1}{2}\left(\frac{\partial u_i}{\partial x_j}\frac{\partial u_j}{\partial x_i}\right)$ (Hunt *et al.*, 1988). Here, $\mathbf{S}$ and $\mathbf{\Omega}$ are the norms of symmetric and antisymmetric components of the velocity gradient tensor $\nabla\mathbf{u} \equiv \frac{\partial u_i}{\partial x_j}$, that is, $S_{ij} = \frac{1}{2}\left(\frac{\partial u_i}{\partial x_j} + \frac{\partial u_j}{\partial x_i}\right)$ and $\Omega_{ij} = \frac{1}{2}\left(\frac{\partial u_i}{\partial x_j} - \frac{\partial u_j}{\partial x_i}\right)$. Positive Q indicates that the vorticity prevails over shear. By definition, Q is the source term in the Poisson equation for pressure $\nabla^2 p = -\frac{\partial u_i}{\partial x_j}\frac{\partial u_j}{\partial x_i} \equiv 2Q$, and the criteria $Q > 0$ indicates the low-pressure regions that can be associated with vortical structures. In planar flows, the condition $Q > 0$ is equivalent to $\lambda_2 < 0$, where λ_2 is the second eigenvalue of $\mathbf{\Omega}^2 + \mathbf{S}^2$ (Jeong & Hussain, 1995). We used the conditions $Q > 0$ and $\lambda_2 < 0$ as large-scale vortical structures identifiers. Figure 8 shows the results. First of all, the regions $Q > 0$ and $\lambda_2 < 0$ overlap. Moreover, on the cross-section $S1$, they overlap with the structure pattern shown in Figure 3.

TURBULENCE STATISTICS

The organized vortical structures in the puff have been revealed by simple time-averaging (Fig. 3), by mwPOD (Fig. 7) and by applying Q- and λ_2-criteria (Fig. 8). To obtain turbulence statistics, we computed the transverse velocity probability distribution function (PDF) and Kurtosis (Ku). The data were collected at 6,084 points on the selected cross-sections (S1, S32 and S63) for 6,000 snapshots, that is, total 36,504,000 data values at each slice. Figure 9 shows color maps of the Kurtosis Ku of the transverse velocity components, u_r (a-c) and u_θ (d-f).

An increase of the Kurtosis can be interpreted as indication of rare events and the intermittent nature of turbulence. Comparing Figures 3a and 9a for radial motion indicates that in the region, that we consider as a large-scale (coherent) structure, Kustosis $Ku \approx 8$, much higher than for a Gaussian distribution. The same but more moderate deviation from the Gaussian $Ku = 3$ we see for the circumfer-

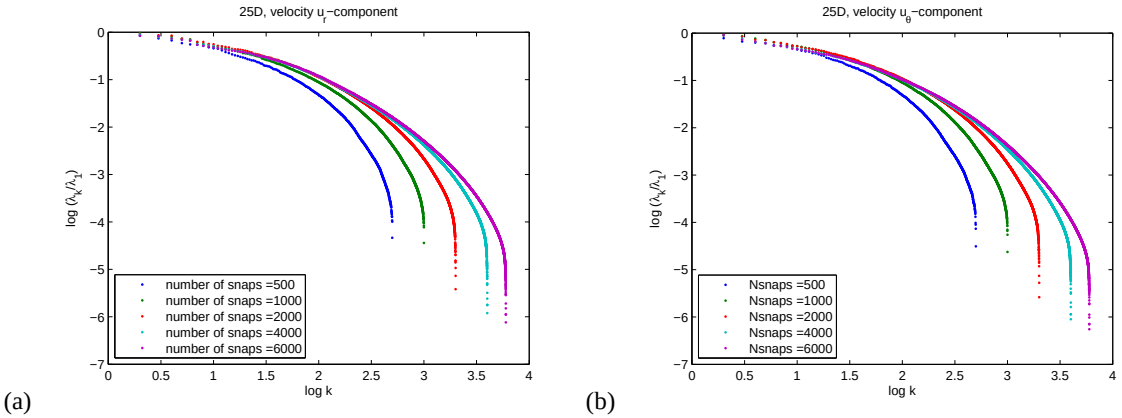

Figure 5. mwPOD: eigenvalue spectra of u_r and u_θ velocity components.

ential u_θ-velocity component (Fig. 9d) where $Ku \approx 5.5$. On the other hand, on the middle cross-section (S32) of moving-window, where the energy of the transverse motion is maximal, the Kurtosis is quite close to the Gaussian, except a high Kurtosis typical for the near-wall region.

In Figure 10, the PDF curve shows a non-Gaussian probability distribution of the fluctuating radial velocity with a spike typical for the intermittent turbulence. Figure 11 shows the PDF very close to the Gaussian for $-3.5 < u'_r/u'_{r,rms} < 3.5$. The deviation from the Gaussian curve relates to the events that take place in the near-wall region. Our results suggest that the radial transport fluctuations in a puff in transitional pipe flow have an intermittent nature.

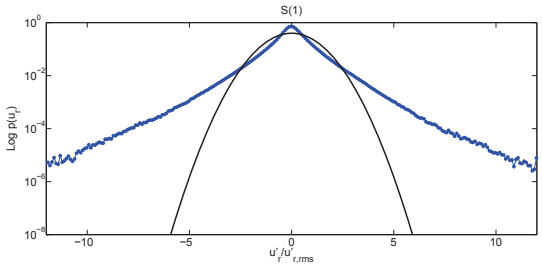

Figure 10. PDF(u'_r) on the cross-section S1; the PDF is centred around a time-averaged value and normalized by $u'_{r,rms}$; solid: Gaussian distribution.

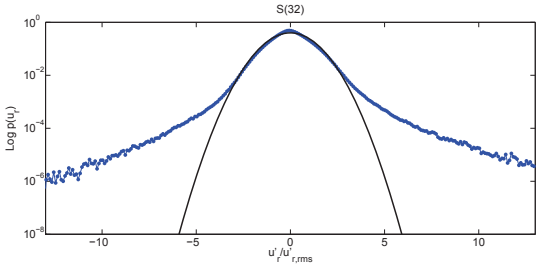

Figure 11. PDF(u'_r) on the cross-section S32; the PDF is centred around a time-averaged value and normalized by $u'_{r,rms}$; solid: Gaussian distribution.

REFERENCES

Avila, K., Moxey, D., de Lozar, A., Avila, M., Barkley, D. & Hof, B. 2011 The onset of turbulence in pipe flow. *Science* **333**, 192–196.

Blackburn, H. M. & Sherwin, S. J. 2004 Formulation of a galerkin spectral elementfourier method for three-dimensional incompressible flows in cylindrical geometries. *Journal of Computational Physics* **197**, 759–778.

van Doorne, C. W. H. & Westerweel, J. 2009 The flow structure of a puff. *Philosophical Transactions of Royal Society A* **367**, 489–507.

Duggleby, A., Ball, K. S., Paul, M. R. & Fisher, P. F. 2007 Dynamical eigenfunction decomposition of turbulent pipe flow. *Journal of Turbulence* **8**, 1–24.

Hunt, J.C.R., Wray, A.A. & Moin, P. 1988 Eddies, stream, and convergence zones in turbulent flows. *Center for Turbulence Research Report CTR-S88*, p. 193.

Jeong, J. & Hussain, F. 1995 On the identification of a vortex. *J. Fluid Mech.* **285**, 69–94.

Moxey, D. & Barkley, D. 2010 Distinct large-scale turbulent-laminar states in transitional pipe flow. *PNAS* **107**, 8091–8096.

Sirovich, L. 1987 Turbulence and the dynamics of coherent structures. part 1: Coherent structures. *Quarterly of Applied Mathematics* **45**, 561–571.

Wygnansky, I. J. & Champagne, F. H. 1973 On transition in a pipe. Part 1. The origin of puffs and slugs and the flow in a turbulent slug. *Journal of Fluid Mechanics* **59**, 281–335.

Wygnansky, I. J., Sokolov, M. & Friedman, D. 1975 On transition in a pipe. Part 2. The equilibrium puff. *Journal of Fluid Mechanics* **69**, 283–304.

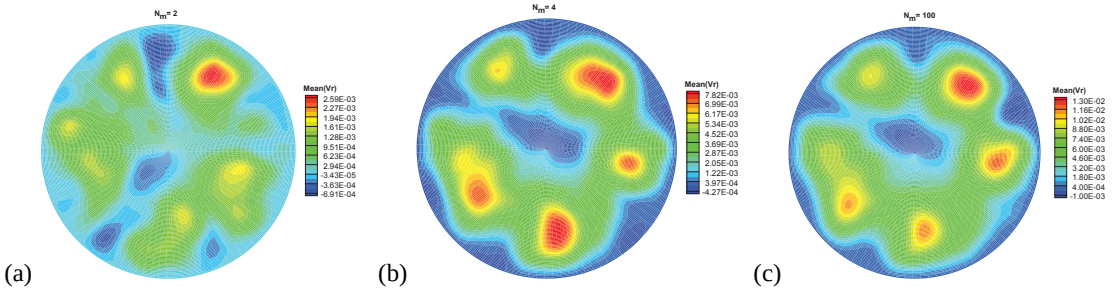

Figure 7. mwPOD reconstructed u_r-velocity field.

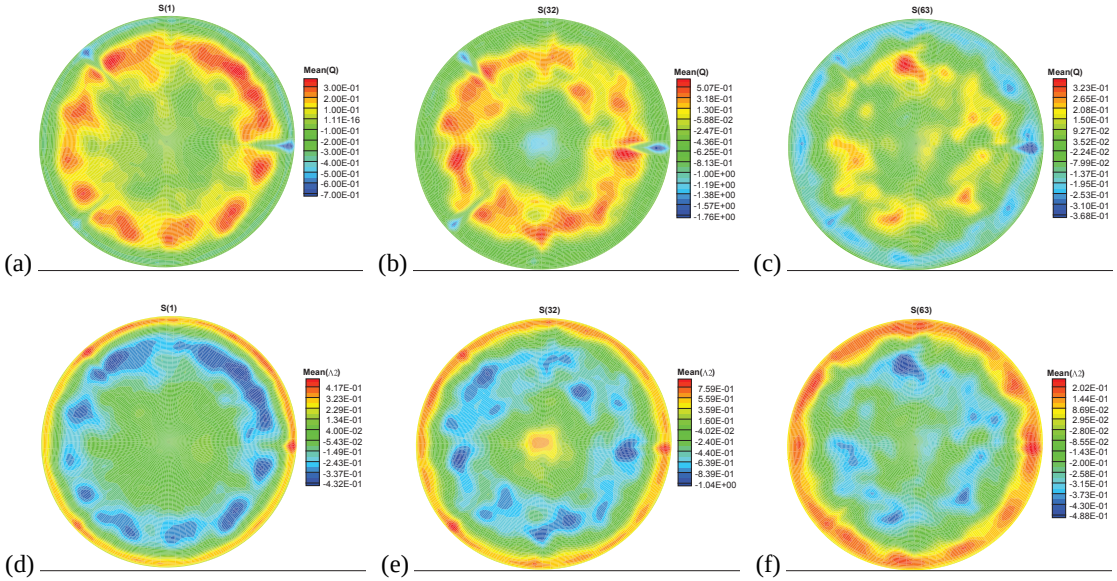

Figure 8. Contours of the second invariant Q (a-c); contours of λ_2 (d-f). S1, S32 and S63 - the trailing edge, middle and leading edge cross-sections, respectively, of a moving-window.

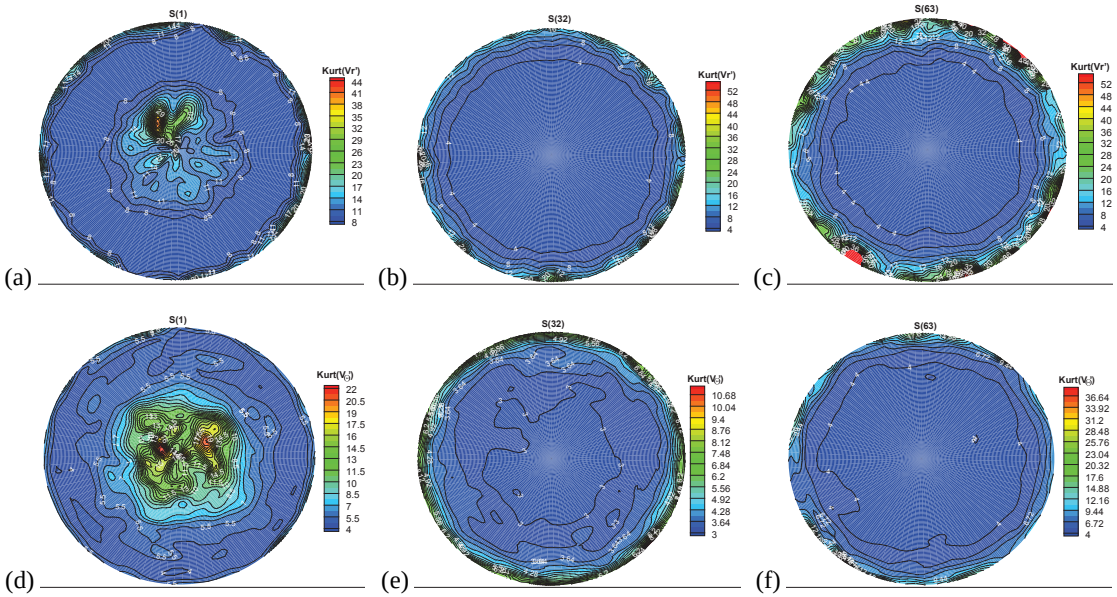

Figure 9. Color maps of the Kurtosis Ku of cross-sectional velocity components, u_r (a-c) and u_θ (d-f). S1, S32 and S63 - the trailing edge, middle and leading edge cross-sections, respectively, of a moving-window.